The Precipitation Characteristics of ISCCP Tropical Weather States

DONGMIN LEE

GESTAR, University Space Research Association, Columbia, and Earth Sciences Division, NASA GSFC, Greenbelt, Maryland, and Seoul National University, Seoul, South Korea

LAZAROS OREOPOULOS

Earth Sciences Division, NASA GSFC, Greenbelt, Maryland

GEORGE J. HUFFMAN*

Science Systems and Applications Inc., Lanham, and Earth Sciences Division, NASA GSFC, Greenbelt, Maryland

WILLIAM B. ROSSOW

Cooperative Remote Sensing Science and Technology Institute, City College of New York, New York, New York

IN-SIK KANG

Seoul National University, Seoul, South Korea

(Manuscript received 7 December 2011, in final form 18 April 2012)

ABSTRACT

The authors examine the daytime precipitation characteristics of the International Satellite Cloud Climatology Project (ISCCP) weather states in the extended tropics (35°S–35°N) for a 10-yr period. The main precipitation dataset used is the Tropical Rainfall Measuring Mission (TRMM) Multisatellite Precipitation Analysis operational product 3B42 dataset, but Global Precipitation Climatology Project daily data are also used for comparison. It is found that the most convectively active ISCCP weather state (WS1), despite an occurrence frequency below 10%, is the most dominant state with regard to surface precipitation, producing both the largest mean precipitation rates when present and the largest percent contribution to the total precipitation of the tropics; yet, even this weather state appears to not precipitate about half the time, although this may be to some extent an artifact of detection and spatiotemporal matching limitations of the precipitation dataset. WS1 exhibits a modest annual cycle of the domain-average precipitation rate, but notable seasonal shifts in its geographic distribution. The precipitation rates of the other weather states appear to be stronger when occurring before or after WS1. The precipitation rates of the various weather states are different between ocean and land, with WS1 producing higher daytime rates on average over ocean than land, likely because of the larger size and more persistent nature of oceanic WS1s. The results of this study, in addition to advancing the understanding of tropical hydrology, can serve as higher-order diagnostics for evaluating the realism of tropical precipitation distributions in large-scale models.

1. Introduction

Cloud processes are crucial to the water and energy cycle. Atmospheric heating rates (due to radiative and thermodynamical processes), surface energy budgets (radiative and turbulent), and precipitation rates have strong dependencies on cloud properties and their

* Current affiliation: Earth Sciences Division, NASA GSFC, Greenbelt, Maryland.

Corresponding author address: Lazaros Oreopoulos, NASA GSFC, Code 613, Greenbelt, MD 20771.
E-mail: lazaros.oreopoulos@nasa.gov

DOI: 10.1175/JCLI-D-11-00718.1

© 2013 American Meteorological Society

Unauthenticated | Downloaded 03/23/22 03:38 PM UTC

frequency of occurrence. While the average effect of clouds can be studied in aggregates, grouping the multitude of observed cloud systems into discernible cloud regimes and studying associated energy and water budgets can be a far more useful approach for understanding the potential impact of cloud changes on future budget distributions. An additional advantage of such a holistic approach is that more physically based diagnostics for evaluating global climate model hydrological and radiative processes can be formulated.

A number of recent studies have focused on the topic of objectively identifying distinct cloud regimes. The criterion commonly used for identifying cloud regimes is the covariation of cloud location (expressed as cloud-top height or pressure) and extinction (expressed as cloud optical thickness or reflectivity). Cloud mixtures exhibiting certain patterns in the covariation of these quantities can be identified as distinct cloud regimes. These patterns emerge from either neural network or *k*-means clustering techniques, with the latter generally being easier to implement and therefore more popular (Jakob and Tselioudis 2003; Rossow et al. 2005; Zhang et al. 2007; Gordon and Norris 2010; Greenwald et al. 2010). The search for patterns can be performed on either a global dataset of joint height-extinction variations or on distinct climatic zones. The breakdown by climatic zone is thought to have the advantage that cloud regime identification can be fine-tuned so that cloud mixtures that may have otherwise been obscured in a larger dataset can emerge in a more geographically targeted analysis. It also allows for examining (dis)similarities between different parts of the globe with regard to the presence and occurrence frequency of different cloud mixtures. With the regimes identified, a variety of properties other than those used to define them can be easily compiled.

A compelling question is whether distinct behaviors of cloud regimes in weather and climate can be established. If the atmospheric conditions under which particular cloud regimes form indeed have identifiable features, it should be possible to associate changes in meteorological conditions with changes in hydrology and energetics through these regimes. Studies along such lines have been conducted in recent years. Several previous studies (Jakob et al. 2005; Williams and Webb 2008; Oreopoulos and Rossow 2011; Haynes et al. 2011) have focused on the radiative characteristics of cloud regimes. Other studies have concentrated on precipitation characteristics. For example, Jakob and Schumacher (2008) combined cloud regimes, inferred from International Satellite Cloud Climatology Project (ISCCP; Schiffer and Rossow 1983) cloud retrievals, with collocated precipitation and latent heating data from the Tropical Rainfall Measuring Mission (TRMM) Precipitation Radar in the tropical western Pacific. By compositing the TRMM precipitation amount and type into the ISCCP regimes, they were able to distinguish between three major precipitation regimes and to identify their surface precipitation rates and latent heat profile characteristics. Tromeur and Rossow (2010) found that while the most convectively active cloud regime dominated by organized deep convection dwarfed the precipitation rate of all other regimes in the $\pm 15^\circ$ latitude zone, the regime representing unorganized convection with a much lower average precipitation rate had nearly the same contribution, because it occurred much more frequently. Lebsock et al. (2010) examined the sensitivities of tropical ocean, top-of-atmosphere radiative fluxes [from Clouds and the Earth's Radiant Energy System (CERES)] to changes in precipitation [from the Advanced Microwave Scanning Radiometer for Earth Observing System (AMSR-E)] for six different cloud regimes derived from Moderate Resolution Imaging Spectroradiometer (MODIS) joint histograms of cloud-top height and optical thickness similar to those by ISCCP. Zhang et al. (2010) defined cloud/precipitation regimes in the tropics from profiles of *CloudSat*/Cloud–Aerosol Lidar and Infrared Pathfinder Satellite Observations (CALIPSO) radar/lidar reflectivities and hydrometeor locations and then compared these with the corresponding regimes of a global climate model operating in weather forecast mode.

In this paper we conduct a more extensive and detailed analysis of the precipitation of tropical ($\pm 35^\circ$ latitude zone) cloud regimes [henceforth referred to as "weather states" (WSs) as in Rossow et al. (2005), who argued about their close association with distinct atmospheric conditions; see also Jakob and Tselioudis 2003; Jakob et al. 2005; Gordon and Norris 2010]. One of our goals is to affirm that the mesoscale weather states identified by ISCCP help in the understanding of tropical precipitation characteristics. We accomplish this by examining the mean magnitude and range of the surface precipitation rate produced by the weather states, their relative contribution to the total precipitation of the tropics, and the geographical distribution of their precipitation. We also seek to further specify the degree to which the most convectively active weather states dominate the tropical precipitation, a topic also investigated by Rossow et al. (2013) using an alternate analysis approach. Our results are featured in section 4, which is broken into subsections that highlight different aspects of the precipitation–weather state relationship. We discuss means, geographical variations, and frequency distributions of each weather state's precipitation rates, and dependencies on the precipitation dataset used. We pay particular attention to the strongest precipitating weather state, specifically its seasonal precipitation variations compared to other convective states, and its close

Unauthenticated | Downloaded 03/23/22 03:38 PM UTC

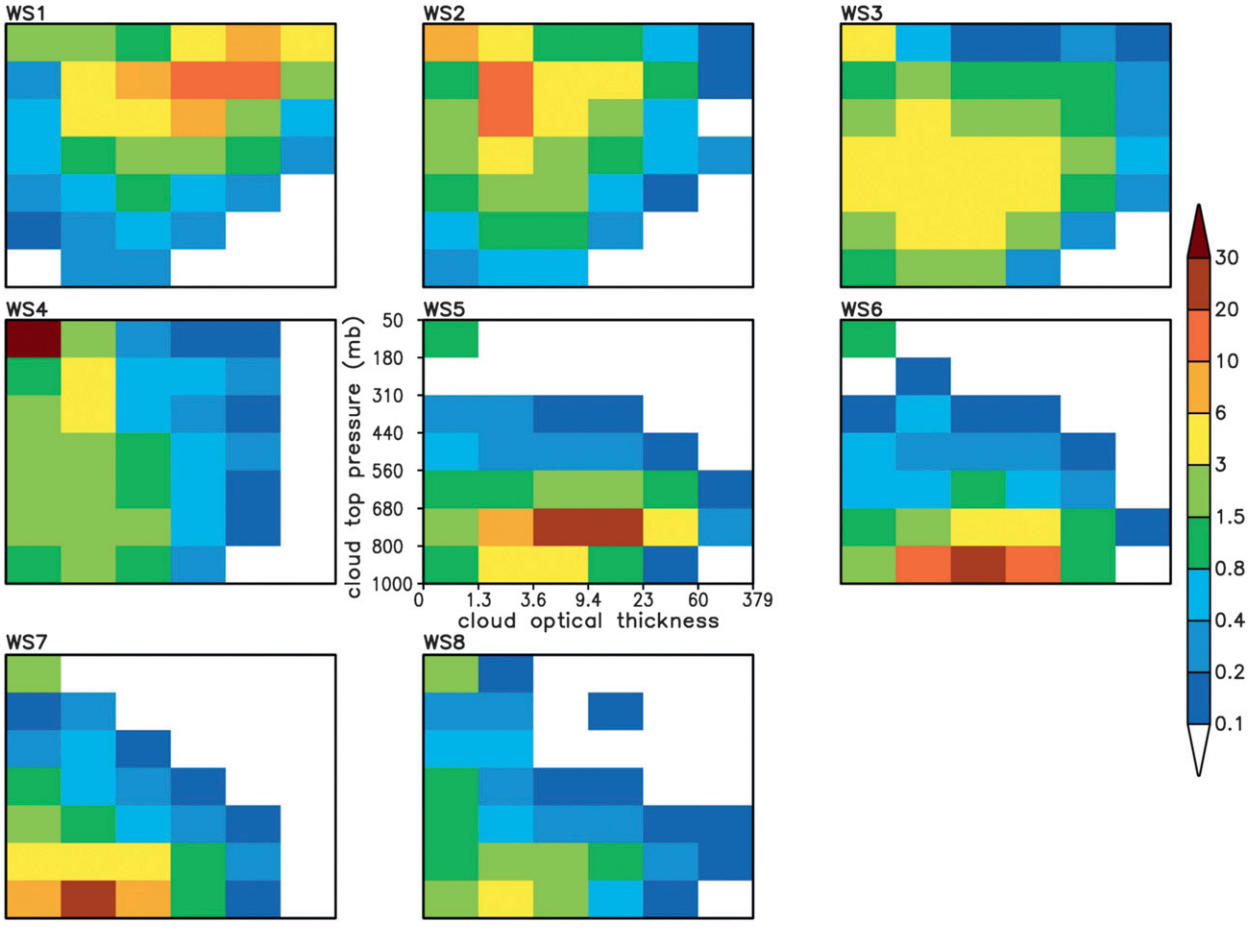

FIG. 1. Cluster centroids for the eight WSs of the extended tropics geographical zone (35°S–35°N) derived from ISCCP D1 data. Each plot shows the normalized frequency of occurrence (in %) within p_c-τ bins. A rough description by the dominant cloud regime is as follows: WS1 corresponds to organized deep convection, WS2 to anvils, WS3 to unorganized deep convection, WS4 to cirrus mixed with some cumulus, WS5 to stratus/stratocumulus, and WS6–WS8 to shallow convection with various degrees of overlying cloudiness and convective intensity.

association with the apparent precipitation of other weather states occurring in close temporal proximity.

2. Datasets used in this study

Our study uses three data sources: the ISCCP weather states for the extended tropics (Oreopoulos and Rossow 2011) to identify cloud regimes, and two precipitation products—the TRMM Multisatellite Precipitation Analysis operational product 3B42 (TMPA-3B42; Huffman et al. 2010) and 1-Degree Daily Global Precipitation Climatology Project (GPCP-1DD; Huffman et al. 2001).

A detailed description of the procedure that generates the ISCCP weather state product is provided by Rossow et al. (2005). Briefly, a search for distinctive patterns is conducted in the joint frequency distributions of cloud-top pressure (p_c) and cloud optical thickness (τ) constructed from individual daytime satellite image pixel retrievals (fields of view about 5 km in size) within 2.5° regions provided in the ISCCP D1 dataset (Rossow and Schiffer 1999). Cluster centroids representing specific histogram patterns describing cloud variability are identified using the "*k*-means" clustering algorithm (Anderberg 1973).

A weather state dataset derived as described above for three geographical zones between 65°S and 65°N is now available for the period 1983–2008. The dataset is available online (ftp://isccp.giss.nasa.gov/outgoing/PICKUP/CLUSTERS/data/1983-2008/). Here, we use the data corresponding to the so-called extended tropical/subtropical zone between 35°S and 35°N, ISCCP dataset D1.WS.ET.dat. This dataset has been previously used by Mekonnen and Rossow (2011) and Oreopoulos and Rossow (2011). The optimal cluster centroids are shown in Fig. 1, while maps of the weather state relative frequency of occurrence (RFO) are provided in Fig. 2. The weather state indexes were assigned according to the classical understanding of expected convective activity strength, with indexes increasing progressively toward

Unauthenticated | Downloaded 03/23/22 03:38 PM UTC

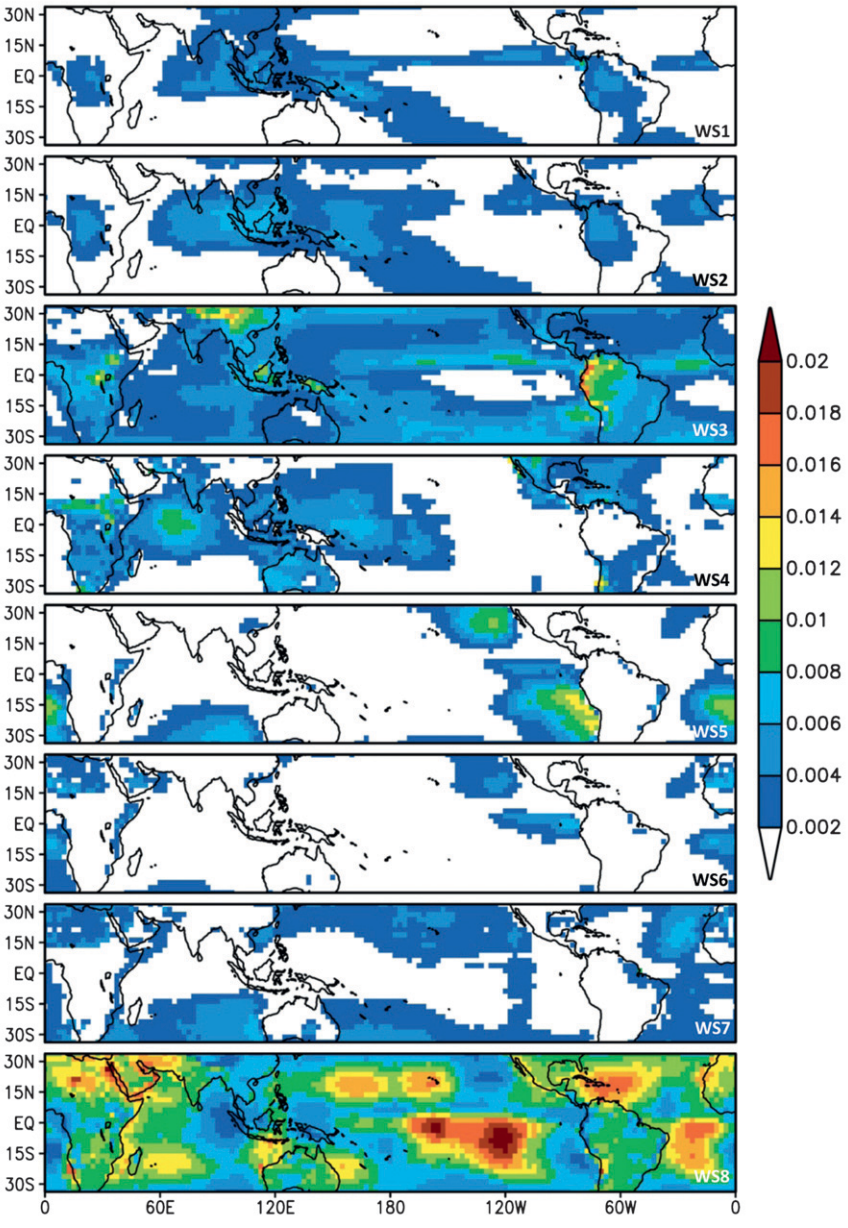

FIG. 2. The geographical distribution of the RFOs of the eight WSs of the extended tropics geographical zone for the period 1998–2007. Values are normalized relative to the total number of WS occurrences with valid TMPA-3B42 precipitation measurements within the geographical area for this period.

the more convectively suppressed weather states. Note that this indexing convention follows Rossow et al. (2005), but is opposite to that of Haynes et al. (2011).

The weather state data are analyzed jointly with two precipitation datasets for a 10-yr overlapping period from January 1998 to December 2007. One is based on the Tropical Rainfall Measuring Mission Multisatellite Precipitation Analysis algorithm, which seeks to provide a ''best'' estimate of quasi-global (50°S–50°N) precipitation from the wide variety of modern satellite-borne precipitation sensors in conjunction with gauge measurements where feasible. Estimates are provided at relatively fine scales, namely 0.25° × 0.25°, 3-hourly (Huffman et al. 2007, 2010). We use the postprocessed research product that relies on calibration by the TRMM Combined Instrument (TCI) product and covers the period from January 1998 to present. The research product system has been developed as the version-6

Unauthenticated | Downloaded 03/23/22 03:38 PM UTC

algorithm for the TRMM operational product 3B42 (3B42 V.6, henceforth TMPA-3B42).

The other precipitation product is the GPCP-1DD version 1.1 precipitation product, which was developed to support the Global Precipitation Climatology Project established by the World Climate Research Programme to quantify multiyear global distributions of precipitation. The product provides 1-day (daily) precipitation estimates on a 1° grid over the entire globe for the period from October 1996 to present. The GPCP-1DD product is a complement to the GPCP version 2 Satellite-Gauge (SG) combination product (Adler et al. 2003). GPCP-1DD uses data from geostationary-satellite infrared sensors to compute the threshold-matched precipitation index (TMPI) and to provide precipitation estimates on a 1° × 1° grid at 3-hourly intervals within the 40°N–40°S latitude zone. The TMPI sequence of instantaneous 3-hourly estimates is summed to produce the daily value. Estimates outside this latitude zone (not used in this study) are computed based on recalibrated Television and Infrared Observation Satellite Operational Vertical Sounder data from polar-orbiting satellites (Susskind et al. 1997). Additionally, the GPCP-1DD product is scaled in both data regions to match the monthly accumulation provided by the SG product, which combines satellite and gauge observations at a monthly time scale on a 2.5° × 2.5° grid.

Although a definitive assessment of the accuracy of the above two precipitation datasets over the full range of precipitation values is not available, it is generally understood that low values of precipitation are often underestimated or missed altogether. The products have nevertheless shown a reasonable agreement in histogram comparisons with surface-based measurements like the Mesonet network of rain gauges in Oklahoma (GPCP-1DD; Huffman et al. 2001) and Precipitation Radar in the western tropical Pacific (TMPA-3B42; Huffman et al. 2010). Although systematic errors (biases) remain a concern, this is not the case for random errors that are negligible because of the large number of data points used in the analysis. For example, for the least frequently observed weather state, WS6, ~2 million precipitating points were available, while for the most frequently observed weather state, WS8, ~17 million precipitating points were analyzed. These large numbers translate to minute errors for the mean precipitation rate, spanning ~0.002–0.01 mm day^{-1} for the full range of weather states.

3. Analysis method

The analysis method is fairly straightforward and basically consists of compositing the precipitation data as a function of the weather state. The D1.WS.ET.dat file contains the weather state index in each 2.5° grid cell for every daytime 3-h interval. Because of their different temporal and spatial resolutions, the two precipitation datasets have to be treated differently in the compositing process. The 3-h resolution of the TMPA-3B42 data allows a certain degree of temporal matching with the ISCCP weather state data that is never worse than 3 h. Spatial matching to the 2.5°-resolution ISCCP weather state data is achieved by taking the mean of all nonmissing (i.e., including zero values) 0.25° precipitation data that fall into the 2.5° grid cell. GPCP data, on the other hand, are resampled from 1° to 2.5° via spatial interpolation.

For each 3-h time period, the TMPA-3B42 data are segregated by weather state to calculate the state's precipitation statistics. However, something analogous cannot be done for the daily averaged GPCP-1DD precipitation data. We therefore pursue two avenues for segregating and compositing GPCP-1DD data: (i) we assign the same daily precipitation rate to all weather states encountered during the daytime period in a grid cell, or (ii) we only consider those grid cells for which the same weather state persists during a day's daylight hours and assign the corresponding GPCP-1DD daily precipitation rate.

Given the above, only TMPA-3B42 composited precipitation can be treated as approaching daytime (i.e., during sunlit hours) precipitation. Because the temporal matching with the ISCCP weather states is better, most of our analysis relies on TMPA-3B42 precipitation data. The availability of GPCP-1DD precipitation rates even without the temporal resolution of TMPA-3B42 still offers, however, useful insight into certain aspects of weather state precipitation, as will be shown below. To have at our disposal two precipitation composites that are more comparable, we also segregate TMPA-3B42 precipitation as in method (ii) of GPCP-1DD compositing, that is, we consider the daily averaged TMPA-3B42 precipitation rates of only those grid cells where the same weather state persists during daytime.

As will be shown in the next section, precipitation data that have been segregated by weather state can be subsequently analyzed in terms of the range and variability of precipitation rates, geographical distributions, relative contributions to the precipitation budget, and other characteristics that help us form a more complete picture about tropical precipitation.

4. Characteristics of tropical weather state precipitation

In this section we identify the relative importance of the various weather states to the tropical precipitation budget, examine the variability of their precipitation rates and the degree to which they are hydrologically distinct, investigate whether a weather state's precipitation is

Unauthenticated | Downloaded 03/23/22 03:38 PM UTC

affected by the state that temporally adjoins it, examine the sensitivity of the results to the precipitation dataset used, and perform an analysis on the seasonal and geographical precipitation characteristics of the three most convectively intense weather states.

a. *Means and geographical distributions of TMPA-3B42 precipitation*

The geographical distribution of the 10-yr TMPA-3B42 daytime precipitation–rate means (including zero rates) at the time of occurrence is shown in Fig. 3 for each weather state. It is immediately obvious that ISCCP joint histogram clustering succeeds in isolating the most intensively precipitating weather state, WS1, representing deep convective regimes with frequent occurrences of high, optically thick clouds (Fig. 1). WS1's mean precipitation rate indeed dwarfs that of any other weather state in the tropics [consistent with the findings of Tromeur and Rossow (2010)], with vast regions of the tropical Pacific and Atlantic Oceans exhibiting mean annual precipitation rates in excess of 25 mm day^{-1}. There are significant regional differences in WS1 precipitation, such as smaller rates over the Indian Ocean and weaker precipitation over land (discussed further below). The mean precipitation rates for the remaining weather states generally decrease monotonically with their assigned index, with WS2 (dominated by convective anvils) and WS3 (representing cloud regimes of frequent unorganized convection) producing significant rates (albeit always lower than 10 mm day^{-1} on an annual basis) consistent with their implicit level of convective activity. From the convectively suppressed states [grouped together in the precipitation frequency histograms of Rossow et al. (2013)] WS4 (dominated by cirrus)–WS8 (shallow convection), WS8 is notable for a stronger precipitation presence over land areas.

To gauge the hydrological importance of a weather state in the tropics, its contribution to the total precipitation of the entire region is also calculated. These results are shown in Fig. 4, as percentage contributions of each weather state to the total gridcell precipitation. Two important points need to be kept in mind when interpreting these figures. First, the contribution of each weather state to the total gridcell precipitation is not only a function of the mean precipitation intensity when the state occurs, but also of its frequency of occurrence in the particular cell. If, for example, one compares the top panel of Fig. 3 with the top panel of Fig. 4 (WS1) there is not much spatial correlation between the mean precipitation rate and contribution. This is because areas where WS1 produces large precipitation rates are often also areas where WS1 rarely occurs. Second, areas where a particular weather state appears to be a major contributor are not necessarily areas where large precipitation totals occur. In other words, the fractional contribution of a state may be large, but with low total gridcell precipitation, the absolute amounts of precipitation involved are small even for the largest weather state contributor. An example of this is WS3 exhibiting a small precipitation amount, but still being the largest contributor of precipitation off the west coast of South America, a generally dry area (Fig. 3). In short, the comparison of Figs. 3, 4 reveals that for precipitation, large averages do not necessarily arise from large-rate events, and that the opposite can also be true; large averages can come from relatively few large-rate events.

The domain-average annual daytime mean precipitation rate and fractional contribution of each weather state to the total tropical precipitation from TMPA-3B42 are shown in Fig. 5. To facilitate the interpretation of the fractional contribution, the domain-average annual RFO is also included in the graph. One can see that despite an RFO of only ~6%, WS1 contributes about half of the total precipitation in the ±35° latitude zone. This is because the mean precipitation rate of ~19 mm day^{-1} for this state is more than 4 times larger than that of the next strongest precipitating weather state (WS2). Still, WS2, along with WS3, is a significant precipitation contributor, collectively contributing about 34% of the tropical precipitation (i.e., about 67% of the precipitation that does not come from WS1). The most frequent state, WS8, with an RFO ~38% contributes less than 8% to the tropical precipitation budget because of its second-smallest (after WS7) mean precipitation rate of ~0.6 mm day^{-1}.

Figure 6 breaks down the results of Fig. 5 into land and ocean domain averages. A 2.5° grid cell is defined as "land" when it contains less than 25% water, "ocean" when it is more than 75% water, and "mixed" in all other cases. According to this convention, 23.1% of 2.5° grid cells in our latitude zone are land, 71.4% are ocean, and the remaining 5.5% are mixed. The most striking finding of the land–ocean breakdown is that the mean precipitation rate of WS1 is significantly higher over ocean (21 mm day^{-1}) than over land (14 mm day^{-1}). This land–ocean contrast is also reproduced when GPCP-1DD data are used in place of TMPA-3B42 (not shown). The difference seems too large to be attributable solely to algorithmic differences in the precipitation retrieval fundamentals over land and ocean, such as the different physics of microwave estimates and the absence of surface gauges over the ocean. A possible contributor to the differences could be the drier environment of continental convection causing the evaporation of a significant fraction of the precipitation before it reaches the ground. This phenomenon, discussed by Geerts and

Unauthenticated | Downloaded 03/23/22 03:38 PM UTC

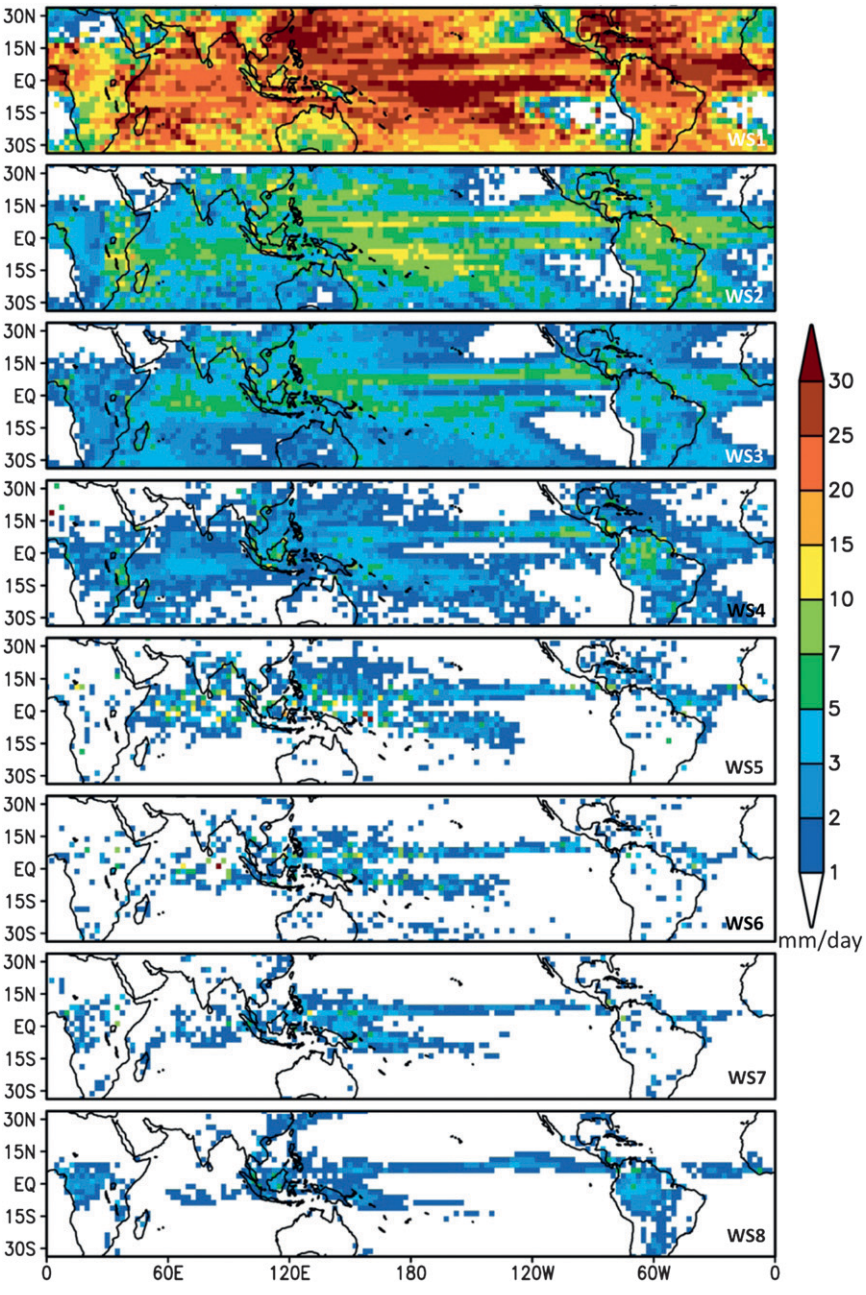

FIG. 3. Geographical distribution of the 10-yr mean precipitation rate (mm day^{-1}) from the TMPA-3B42 dataset for each of ISCCP's eight extended tropics WSs.

Dejene (2005), who noted radar reflectivity profiles peaking at high altitude and decreasing toward the ground in Africa, would be captured by the TMPA-3B42 and GPCP-1DD datasets because of the surface gauge rescaling employed.

We believe, however, that the main reason for the land–ocean contrast in WS1 precipitation rates is that the oceanic WS1 systems are bigger and slower (e.g., Machado and Rossow 1993; Hodges and Thorncroft 1997; Machado et al. 1998), thus producing greater mean precipitation rates even if less intense locally. To investigate the possibility of bigger oceanic WS1 systems, we examined whether fewer (compared to continental WS1) TMPA-3B42 zero values contributed to the 2.5° gridcell precipitation rate value, the underlying assumption being that fewer zeros indicate larger systems. We found that this was indeed the case, and furthermore, when the tropical domain WS1 average was calculated from only

Unauthenticated | Downloaded 03/23/22 03:38 PM UTC

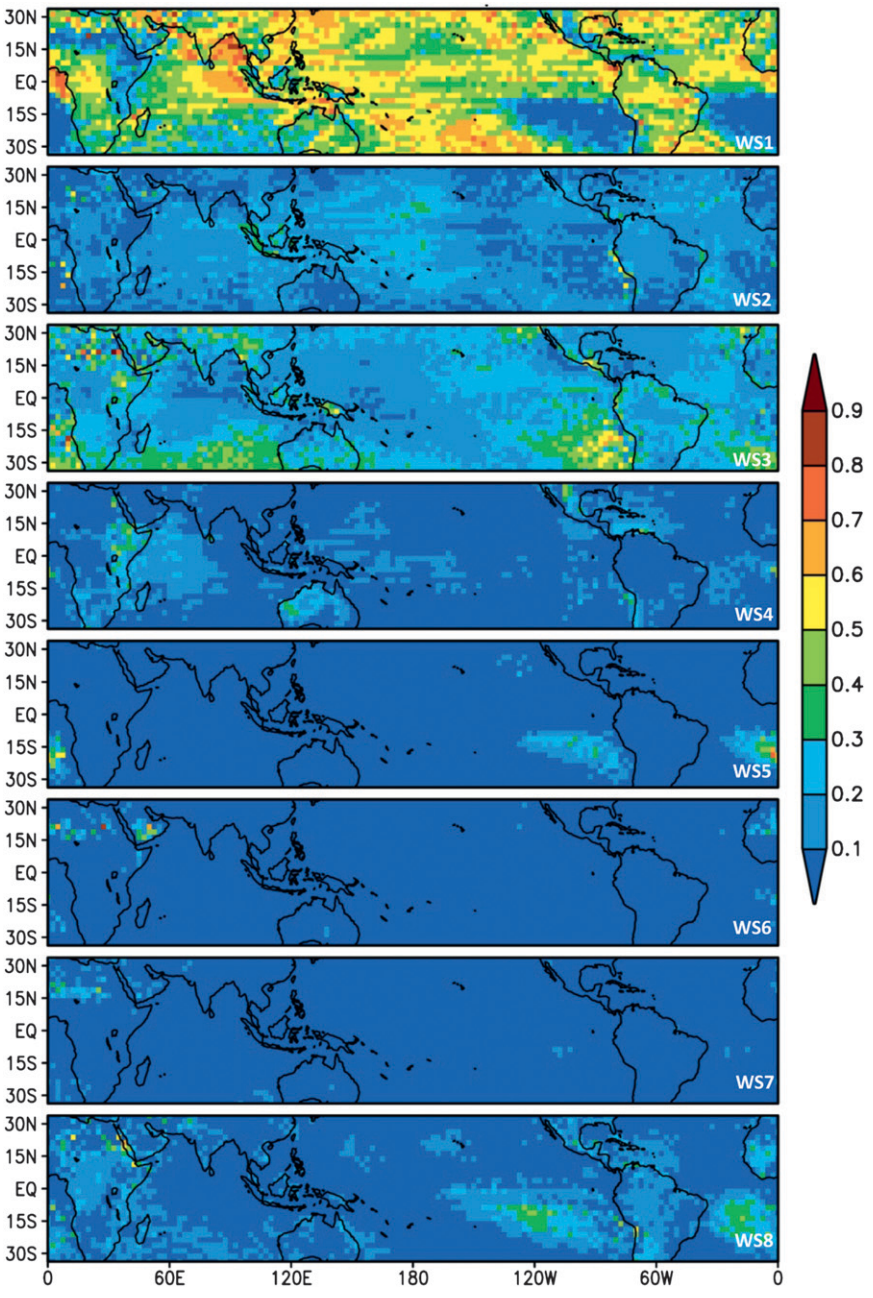

FIG. 4. Geographical distribution of the fractional contribution to the total 10-yr TMPA-3B42 gridcell precipitation of each ISCCP extended tropics WS.

nonzero TMPA-3B42 precipitation values, the oceanic and continental daytime mean precipitation rates were very similar (not shown). For WS2 and WS3 we actually found larger means over land than ocean by employing this selective averaging of nonzero TMPA-3B42 values. So, it appears that precipitation from convective systems (WS1 + WS2 + WS3) is locally stronger over land, but is also spatially more confined. We also examined the ''slowness'' of WS1 in terms of temporal persistence. We calculated the relative likelihood that if a weather state appears in a grid cell at a certain time, the same state will again be encountered in the same grid cell 3 or 6 h later (Fig. 7). We carried out the analysis separately over land and ocean and found that for both 3- and 6-h lags, the relative frequency of situations where WS1 persists is greater for ocean than over land (negative values for the WS1–WS1 pair in Fig. 7), indicating longer-lasting (slower) systems over ocean. It is worthwhile noting that

Unauthenticated | Downloaded 03/23/22 03:38 PM UTC

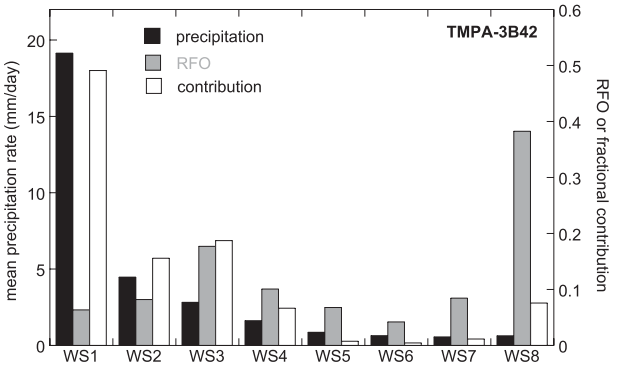

FIG. 5. Domain-average values of the mean precipitation rates and fractional contributions shown in Figs. 3, 4. Also included is the domain-average RFO of each WS.

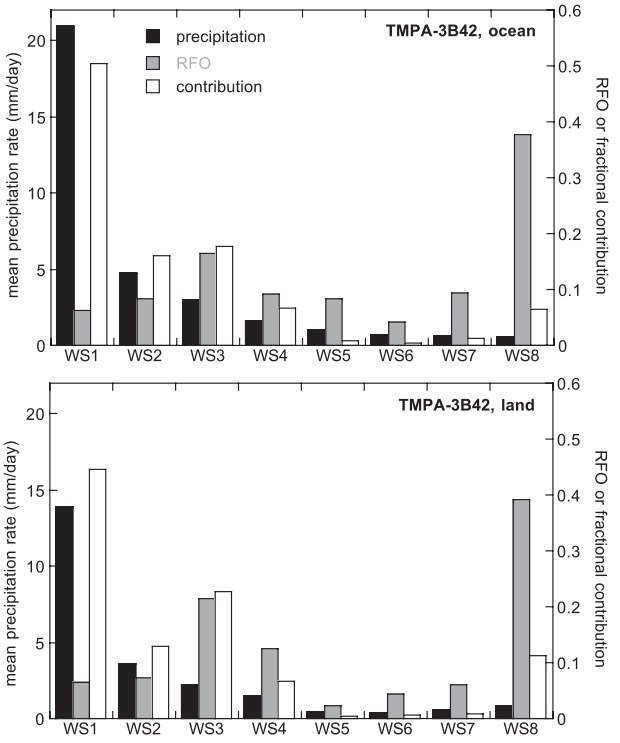

FIG. 6. As in Fig. 5, but when TMPA-3B42 precipitation is aggregated separately over (top) ocean and (bottom) land.

it is WS2 for which the relative persistence contrast between land and ocean is the most pronounced, while for WS3 persistence is smaller than in either WS1 or WS2.

Returning to Fig. 6, we also see that while the ranking of the weather states with respect to their contribution to the total precipitation is not different between ocean and land, the relative contribution of the different weather states to the continental or marine precipitation budget exhibits some changes compared to the overall values. For example, WS1 is a larger fractional contributor to ocean precipitation than land precipitation, the opposite is true for WS8, and WS2 and WS3 are more on par in ocean precipitation contribution than in land precipitation contribution. Differences in the relative fractional contribution between land and ocean can be the combined outcome of changes in both mean precipitation intensity and RFO. For WS1 we see that the RFO over ocean and land is about the same (0.062 and 0.065, respectively) and the main factor making WS1 a larger relative contributor over ocean is mean WS1 precipitation rate being greater in oceanic grid cells. In the case of WS3, where both the mean precipitation and the RFO are substantially different between land and ocean, but in opposite directions, it appears that the greater RFO over land dominates the fractional contribution.

b. *Comparisons between different datasets and compositing approaches*

We now examine global values of mean precipitation rate and contribution when daily averaged GPCP precipitation is composited. Because of the coarser temporal resolution of the GPCP dataset, additional assumptions have to be employed for compositing, as explained earlier. The comparison between TMPA-3B42 and GPCP-1DD weather state precipitation is shown in Fig. 8. The top left panel of this figure is the same as in Fig. 5, which shows the domain-average daytime mean rate and contribution to the total precipitation from our best compositing method of TMPA-3B42 data always temporally matched within 3 h with ISCCP weather state data. The other panels show results using the alternate compositing approaches discussed in section 3, necessitated by the daily average nature of the GPCP-1DD dataset. The upper right panel shows domain-average values obtained by assuming that the GPCP-1DD precipitation is constant throughout the day: all weather states identified during the sunlit period of a grid cell are assigned the same value of precipitation, namely the (spatially interpolated to 2.5°) daily average provided by GPCP-1DD. The lower left panel shows values obtained using only those grid cells for which the same weather state persists during the day's daylight hours. Presumably, for the grid cells satisfying the single–weather state condition, the assumption of a constant precipitation rate will be acceptable to some degree. Note that close to the international date line daylight hours may be split between two UTC days containing GPCP-1DD data, so this area is underrepresented in this form of conditional compositing. In the lower right panel, the TMPA-3B42 data are composited the same way, that is, using the daily averaged TMPA-3B42 precipitation and only those grid cells with occurrences of a single weather state during the entire sunlit period.

Unauthenticated | Downloaded 03/23/22 03:38 PM UTC

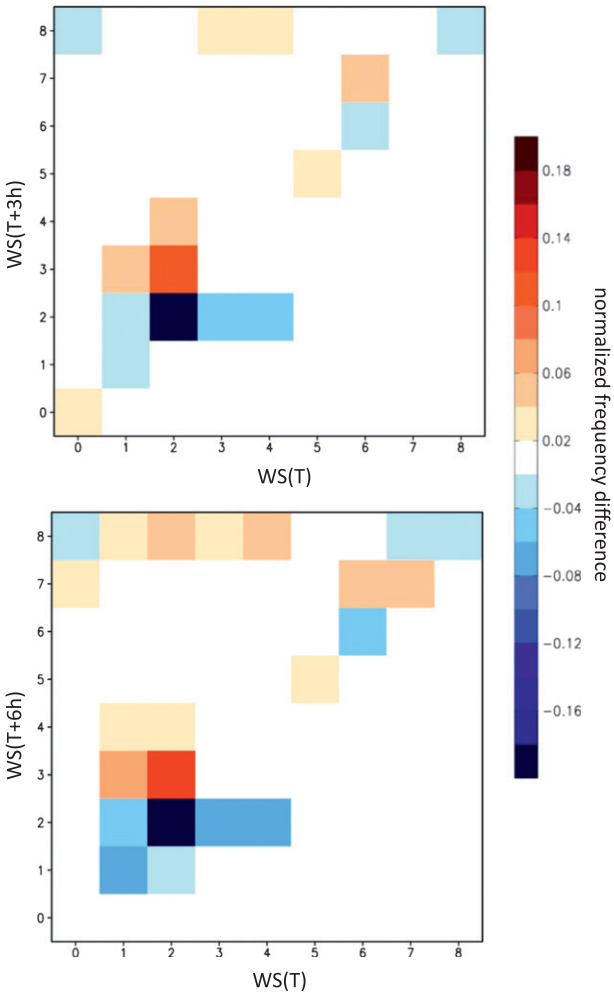

FIG. 7. Difference from TMPA-3B42 in the relative likelihood of occurrence between land and ocean (negative numbers indicate that likelihood is larger over ocean) of a particular WS occurring at (top) 3 h (T + 3h) or (bottom) 6 h (T + 6h) when another WS occurs at time T. Our focus is on transitions between identical states, represented by the values on the diagonal.

The RFOs are comparable between the top panels of Fig. 8 that use all weather state data and the bottom two panels that use only the fraction of grid cells with the same persistent weather state throughout the daytime. The RFOs of the bottom panels increase relative to those of the top panels for the states that have the largest fractions of grid cells with a persistent daytime weather state. This is most notable for WS8 (shallow convection with frequent occurrences of overlying clouds), which has an RFO of 0.383 when all the grid cells are accounted for and an RFO of 0.528 when only the grid cells with no daytime variability of weather state occurrence are considered. Indeed, for WS8 the fraction of grid cells of the latter type is 18.4%, larger than the counterpart fraction of any other weather state. On the other hand, the RFO of (weakly precipitating) WS7 (mostly subtropical oceanic shallow convection) drops from ~0.085 to 0.039 when implementing this screening because only 6.3% of grid cells (lowest of all weather states) containing WS7 maintain this weather state for the entire daytime period; in other words, WS7 rarely persists during the daytime in the tropics. Overall, the fraction of grid cells with a single weather state during daytime is about 13%; that is, about 87% of data are discarded to produce the bottom panels of Fig. 8.

Contrasting the top panels reveals that using the GPCP-1DD data and the constant daytime precipitation assumption leads to a notably different picture of the precipitation intensity and relative importance of the three most convective states, compared to TMPA-3B42. The precipitation rate of WS1 falls from ~19 to ~14.5 mm day^{-1} and the fractional contribution from 0.49 to 0.33. In contrast, the mean precipitation rate and fractional contribution of WS2 and WS3 increase: the ratio of WS2 and WS1 fractional contributions increases from 0.32 for TMPA-3B42 to 0.60 for GPCP-1DD, while the ratio of WS3 to WS1 fractional contributions increases from 0.38 to 0.68. It appears therefore that when WS2 or WS3 are observed in a grid cell on the same day as WS1, the constant daytime precipitation assumption assigns to WS2 and WS3 daily averaged precipitation estimates inflated by the occurrence of WS1 in the hours before or after (this is further examined later). One can of course view this mistaken assignment of precipitation also from the WS1 perspective, with weaker precipitation assigned to WS1 in grid cells where convectively weaker states have also occurred during the same day. Such misassignments also seem to be "benefiting" the convectively suppressed states WS4–WS8, making them appear as somewhat stronger precipitation producers and contributors according to GPCP-1DD compared to TMPA-3B42.

As pointed out earlier, one can attempt to bring the two precipitation datasets to a more equal footing by including in the compositing only the grid cells with a single weather state during daytime. The results from this analysis are shown in the bottom panels of Fig. 8. The domain-average annual precipitation rates and fractional contributions from the two satellite datasets look in this case more similar when partitioned by ISCCP weather state. Some differences remain, such as the different relative contribution strengths of WS2 and WS3, which are closer in GPCP-1DD than TMPA-3B42, but the chief finding, WS1's dominance, has now been restored in GPCP-1DD to the same level as in TMPA-3B42.

The above analysis confirms the substantial daytime variations in tropical precipitation indicated by previous studies (e.g., Nesbitt and Zipser 2003). These variations

Unauthenticated | Downloaded 03/23/22 03:38 PM UTC

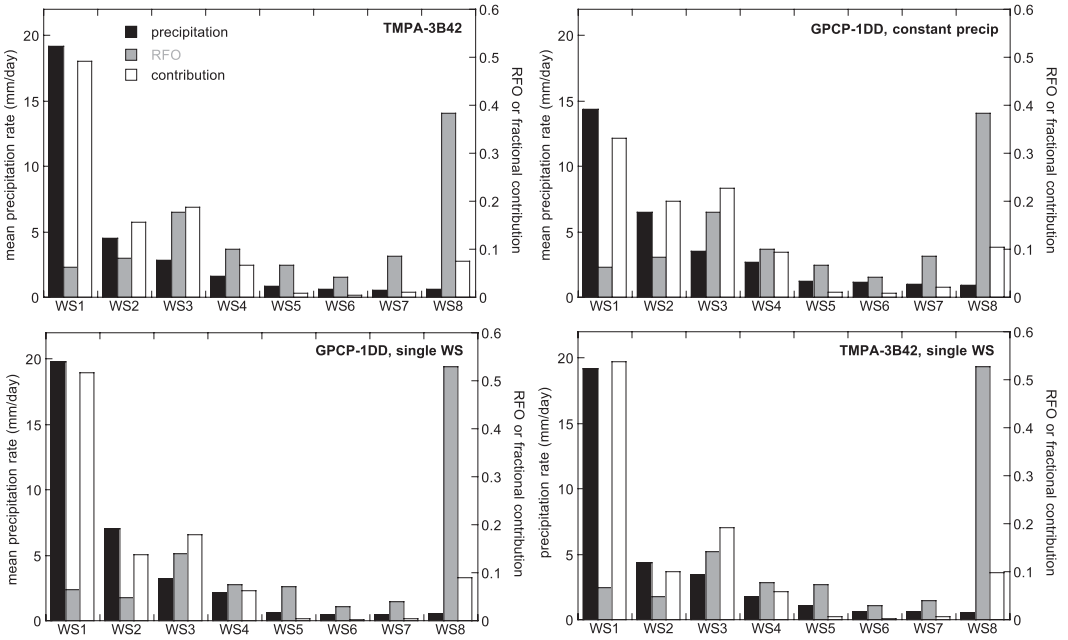

FIG. 8. (top left) As in Fig. 5. (top right) As in (top left), but using GPCP-1DD precipitation rates, assumed constant throughout the day. (bottom left) As in (top right), but using only those grid cells with the same WS occurring during daytime. (bottom right) As in (top left), but with precipitation diurnally averaged for those grid cells with the same WS persisting during daytime.

can affect the outcome of compositing a daily averaged product like GPCP-1DD to a considerable extent.

c. *Distributions of weather state precipitation rates*

So far we have been examining only the mean annual precipitation of the ISCCP weather states either on a domain average or regional scale. We will now attempt to gain a better understanding of the range and variability of a state's precipitation using cumulative precipitation-rate histograms. Rossow et al. (2013) discuss in detail other ways of constructing conditional precipitation histograms and their dependence on spatial gridding.

Four sets of cumulative histograms are shown in Fig. 9, with each panel corresponding to the same dataset and compositing assumptions as in Fig. 8. The cumulative frequencies are normalized relative to the number of each state's occurrences. The first bin is considered nonprecipitating and includes all precipitation values below 0.048 mm day^{-1}, the lowest precipitating value in the original spatial resolution TMPA-3B42 dataset.

Once again, the top left panel of Fig. 9, based on TMPA-3B42, corresponds to the best possible temporal matching between weather state identification and precipitation. The first, perhaps surprising, feature seen in this panel is that even the strongest precipitating state, WS1, about half the time is not precipitating according to TMPA-3B42. This large fraction of nonprecipitating deep cloud systems, although consistent with previous work like Casey et al. (2007), is probably an overestimation given the inherent weakness of the algorithm in detecting light precipitation and our inability to achieve exact spatiotemporal matching with the datasets at hand. But even if not as pronounced in the real world, the frequent occurrence of apparently nonprecipitating WS1 cloud systems reminds us that the ISCCP weather states are only statistical descriptions of cloud regimes that encompass a substantial variety of cloud mixtures. These mixtures may include clouds with significantly higher and lower than average cloud-top pressures and optical depths, respectively, than the WS1 centroid, that are yet more closely related to that cluster centroid than any of the others. A cursory analysis with 1 yr of ISCCP D1 data indicated that the average cloud-top pressure and cloud optical depth of grid cells containing WS1 was 317 hPa and 10.6 when TMPA-3B42 indicated no precipitation and 291 hPa and 13.5 when precipitation was detected. This finding suggests significant height and extinction differences between nonprecipitating and precipitating WS1s. Variability among tropical WS1s has also been implied in the results of Fig. 6 in Oreopoulos and Rossow (2011) showing very wide WS1 shortwave and longwave cloud radiative effect histograms. Finally, as indicated earlier, some zero-precipitation WS1 occurrences may be due to space and time mismatches: TRMM obtains an instantaneous sample within a 3-h period and so does ISCCP, but they do

Unauthenticated | Downloaded 03/23/22 03:38 PM UTC

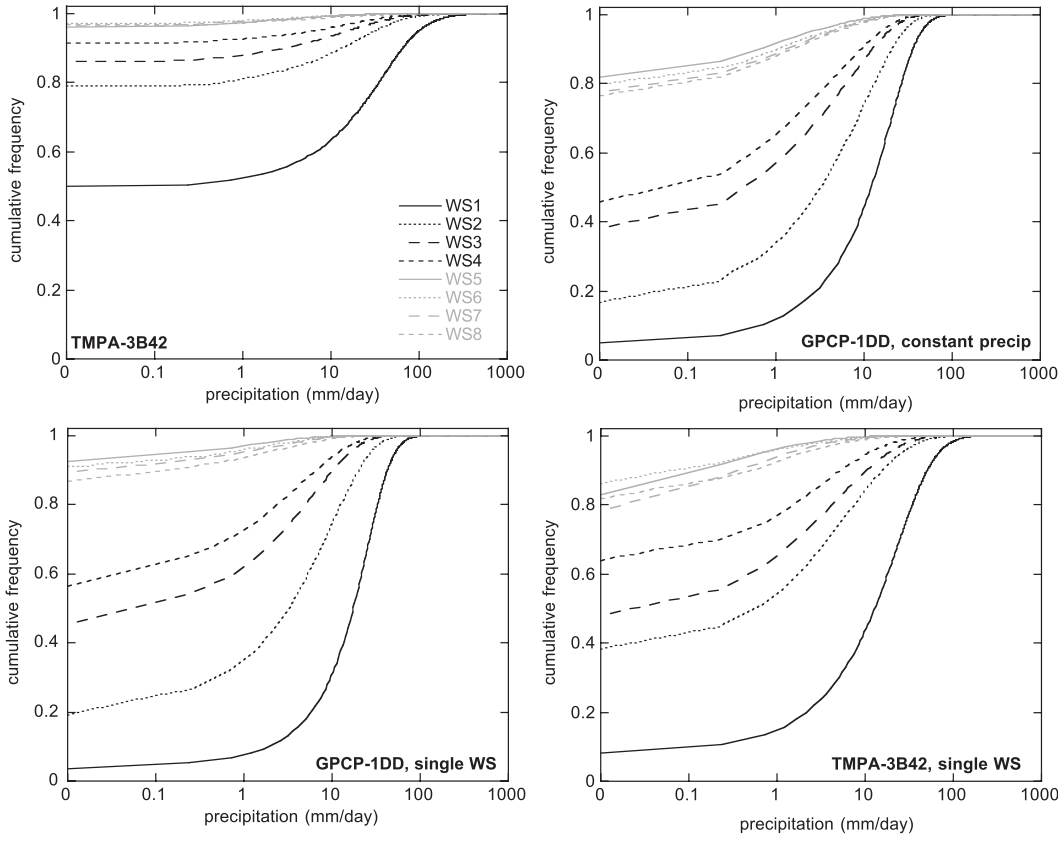

FIG. 9. Cumulative histograms of precipitation rate for each WS for the precipitation datasets and compositing assumptions used in Fig. 7.

not necessarily coincide within that time interval, with possible separations of up to almost 3 h. Likewise, because the ISCCP data are spatially sampled at 30 km, and TRMM may not be looking at the same pixels, different areas within the same grid cell may be captured by the two datasets. Consider, for example, that in the WS1 centroid of Fig. 1, ~70% of p_c–τ joint frequencies occur at $p_c >$ 440 hPa and $\tau < 23$ (i.e., outside the convective core) and that TRMM observations may often be collocated with ISCCP observations belonging to this much less likely to precipitate portion of the joint histogram.

The fraction of nonprecipitating WS1 occurrences drops dramatically when daily averaged precipitation values are used (top right and bottom panels of Fig. 9). This indicates that when WS1 appears in a grid cell at some point during daytime, it is very likely that precipitation will occur at some time during the same day. Indeed, regardless of what dataset or assumption is used for compositing daily precipitation, there is never a higher than 10% chance that a grid cell containing WS1 will remain precipitation-free for the entire day. An encouraging indicator of the consistency of our analysis is the fact that despite the completely different shape of the WS1 TMPA-3B42 cumulative histograms in the upper left and lower right panels of Fig. 9, the resulting mean precipitation rates (upper left and lower right panels of Fig. 8) are very close.

The frequency of nonprecipitating cloud mixtures (with the spatiotemporal matching caveats mentioned above) increases rapidly as one progressively moves to the most convectively suppressed weather states. For example, even for WS3, 86% of occurrences are not associated with any precipitation according to TMPA-3B42 (upper left panel of Fig.9). These frequencies are again smaller when daily precipitation averages are composited: the other three panels agree that only ~45% of grid cells containing WS3 at some point during daytime will remain precipitation-free throughout the day.

At the high end of the precipitation distribution we note from the top panel of Fig. 9 that while about 26% of WS1 occurrences are associated with rain rates above 24 mm day^{-1}, the corresponding percentage drops to about 7% for WS2, 4% for WS3, and more rapidly thereafter to values below 0.5% for WS5–WS8. This part of the histogram is changed less by the details of compositing. For

Unauthenticated | Downloaded 03/23/22 03:38 PM UTC

example, the top right panel based on GPCP-1DD has counterpart values for WS1–WS3 of 23%, 7%, and 3%, indicating that strong precipitation also tends to be persistent. The cumulative histograms of the last four weather states form a group of histogram curves that is clearly distinct from the other states, also characterized by well-separated histograms. This is another piece of evidence supporting our claim that the ISCCP weather states are good classifiers of the various tropical precipitation regimes.

d. Dependence of precipitation on weather state transitions

Another approach for assessing precipitation variability within weather states is to examine whether a weather state's precipitation correlates with which state precedes or follows it. Intuitively, one would expect some correlation because a particular state's realization may have features that depend on the state that precedes or follows and we have a limited ability to spatiotemporally match the datasets. For example, a cloud mixture classified as WS3 may have different features when it follows WS1 instead of (probably more rarely) WS2 and may be assigned some of the TMPA-3B42 values that actually belong to WS1.

Figure 10 shows the annual domain-averaged precipitation of a weather state as a function of the weather state that either precedes (top panel) or follows (bottom panel). Such an analysis can obviously only be performed with the 3-hourly TMPA-3B42 dataset. For all weather states, the mean precipitation rate is stronger when the state is preceded or followed by WS1 (second column from left). The frequency with which transitions to or from WS1 happen is, of course, different for each weather state and does not affect the values in the figure, which simply correspond to the mean precipitation rates when the state occurs. Interestingly, except for the case where it is preceded or followed by itself, WS1 exhibits the strongest precipitation when it is preceded or followed by WS8 than any other case (second row from bottom), including the ones that are convectively stronger. The transition from WS8 to WS1 and vice versa is, however, rare (not shown). One other interesting feature seen in the bottom plot is that the mean precipitation of WS2, WS3, and WS4 falls within the same range of 9–12 mm day^{-1} when followed by WS1. This is especially surprising for WS4, which is a rather weakly precipitating state when the analysis is not conditional on close temporal proximity to WS1. But when WS1 precedes, WS2 precipitates more than WS3 or WS4 (top plot). These transition results make sense considering the fact that the changing weather states simply represent different parts of the same storm system and the possible temporal and spatial mismatches between ISCCP weather state and TMPA-3B42 precipitation.

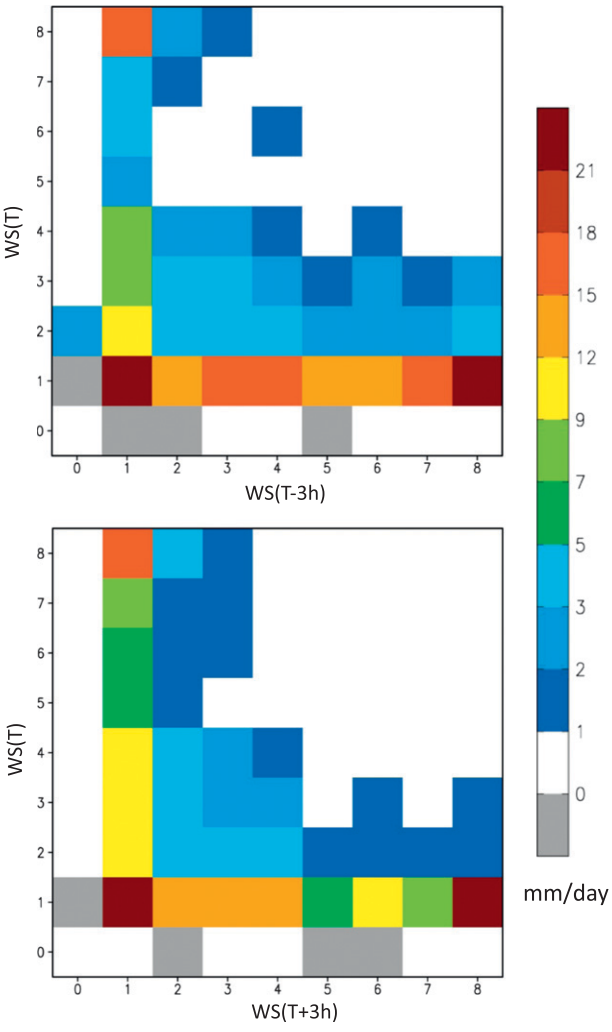

FIG. 10. Mean TMPA-3B42 precipitation rate of each WS (with "0" designating cloud-free 2.5° cells, and gray squares indicating nonexistent combinations) at time T as a function of the WS either (top) 3 h earlier ($T - 3$h) or (bottom) 3 h later ($T + 3$h).

The great influence of transitions to or from WS1 can also be quantified by examining the combined domain-average precipitation rates of all weather states except WS1. This domain average is 1.56 mm day^{-1} in the general case where the specifics of the preceding or succeeding weather state are ignored, and 8.16 and 10.71 mm day^{-1} when WS1 precedes or succeeds any of these weather states. Because of their lower values, the precipitation characteristics of other combinations of weather state transitions are inconsequential and are therefore not discussed.

e. Seasonal variations of the most convective weather states

Our analysis so far has clearly demonstrated that WS1 is by far the most important weather state for tropical

Unauthenticated | Downloaded 03/23/22 03:38 PM UTC

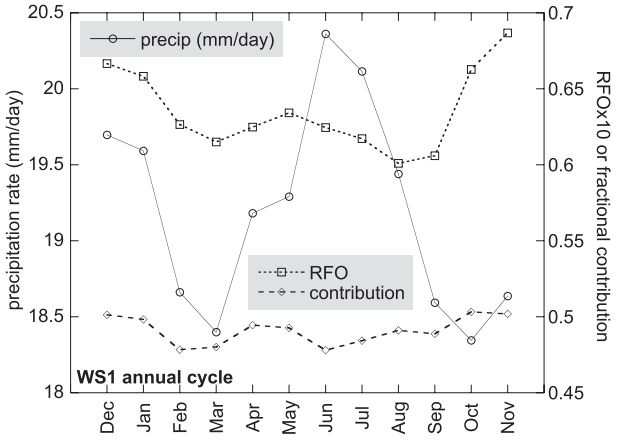

FIG. 11. The 10-yr mean annual cycle of WS1 TMPA-3B42 precipitation rate when present, fractional contribution to domain precipitation, and RFO.

precipitation, affirming the dominance of organized (WS1) over single-plume deep convection (WS3) also shown in Rossow et al. (2013). In this subsection we perform additional analyses of WS1 precipitation characteristics, focusing on seasonal and zonal variations and how they contrast with their counterpart features in WS2 and WS3. The seasonal variations of the other states' precipitation were also examined but are not shown because both the precipitation rates themselves and their relative seasonal variability are appreciably weaker. From a domain-average perspective, even the WS1 annual cycle of mean precipitation is not particularly strong (Fig. 11), a result also found by Tselioudis and Rossow (2011). The maximum value occurs in June, but is only ~6% higher than the annual mean; the minimum value occurs in March, but is only ~4.5% below the annual mean. Seasonal variations in the fractional contribution relative to the annual mean are yet lower (2.5% above the annual mean in October and 2.7% below the annual mean in June are the highest deviations). This is because months with relatively high precipitation rates also have relatively low RFOs and vice versa. The seasonal cycles of the domain-average WS2 and WS3 precipitation rate and fractional contributions are even weaker (not shown).

Even though the seasonal variations of domain-average WS1 precipitation are not strong, geographical distributions vary significantly with season. Figure 12 shows the zonal averages of total precipitation for the three most convective weather states—WS1, WS2, and WS3—in four seasons [December–February (DJF), March–May (MAM), June–August (JJA), and September–November (SON)], normalized by their respective domain-average annual mean. This type of normalization illustrates not only seasonal deviations from the annual mean, but also

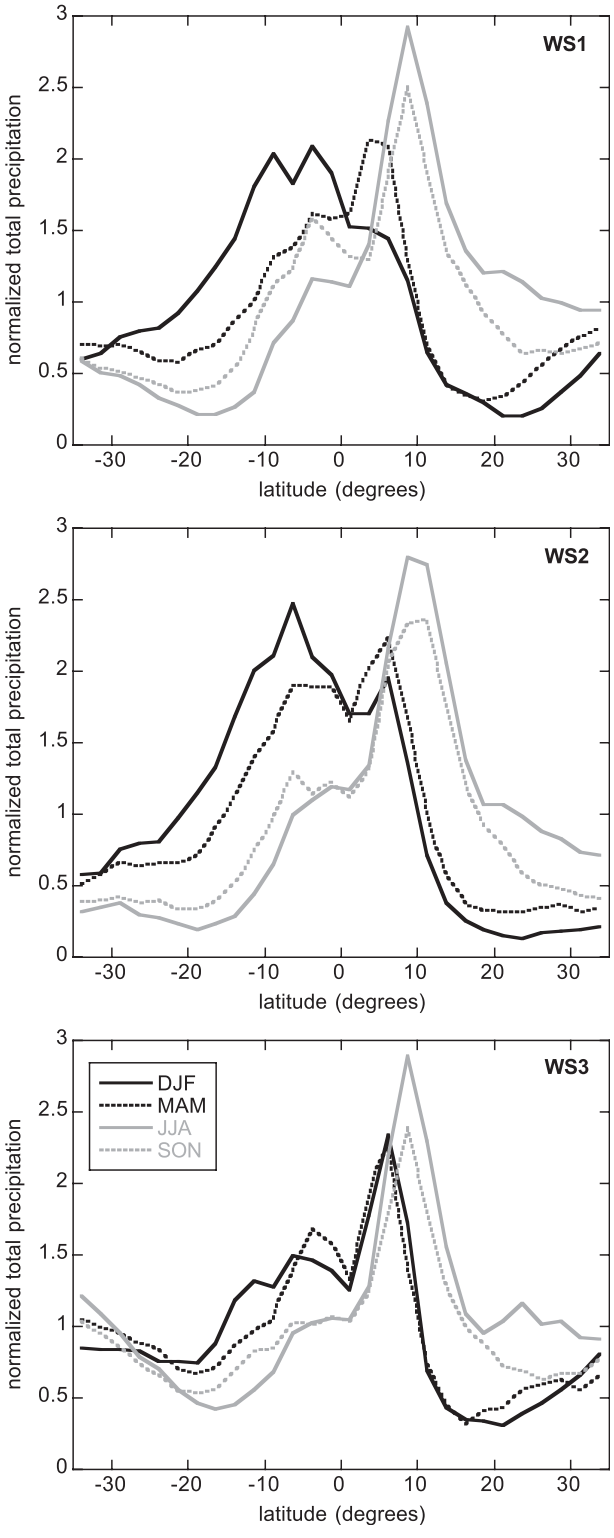

FIG. 12. Seasonal variability of total zonal precipitation normalized by the domain-averaged annual mean for (top) WS1, (middle) WS2, and (bottom) WS3.

Unauthenticated | Downloaded 03/23/22 03:38 PM UTC

geographical (zonal) deviations from the domain average. There are substantial zonal movements of WS1 precipitation in accordance with movements of WS1 occurrence (not shown). The band of deep convection known as the ITCZ moves northward from DJF to JJA and this is reflected in the northward displacement of normalized WS1 and WS2 precipitation totals. This is not the case for WS3, which exhibits little zonal movement as seasons vary, although some seasonal changes in specific areas such as India and Southeast Asia take place (not shown). When seasonal maps of WS1 precipitation were examined (not shown), we noted that this weather state produces the lowest precipitation totals over Africa and South America in JJA and the highest precipitation totals over South Asia, including India and the Bay of Bengal. The eastern equatorial Pacific WS1 precipitation was also stronger during JJA. DJF marked the return of WS1 precipitation south of the equator in Africa and South America, and high precipitation totals were encountered in the South Pacific convergence zone and the western part of the Maritime Continent where WS1 occurrence peaks. Thus, while WS1 (and WS2) precipitation totals for the entire geographical zone do not change by much, the zonal and meridional precipitation movements are quite prominent and are the main drivers of seasonal variability in overall tropical precipitation. On the other hand, for WS3, in addition to the domain average that does not change much with season, the zonal structure remains relatively unchanged as well.

5. Summary and discussion

We provide a comprehensive picture of the relationship between ISCCP weather states (also called cloud regimes by some authors) and precipitation for the entire tropics (35°S–35°N), thus significantly expanding upon prior studies that were geographically more limited. Our analysis relies on the concepts of conditional sampling/sorting and composite averaging. By employing these concepts on two widely used merged (satellite and surface) precipitation datasets, TMPA-3B42 and GPCP-1DD, we gain insight on how the tropical precipitation budget is partitioned among the various weather states identified by analyses of ISCCP-retrieved cloud properties. We focus primarily on the TMPA-3B42 precipitation dataset because it has the same 3-h temporal resolution as the ISCCP weather states. Given that weather states can only be identified during daytime when cloud optical thickness from passive visible observations is available, our findings, based on 10 yr of measurements, only apply to daytime precipitation. Compositing of GPCP-1DD data, on the other hand, can be performed only on diurnally averaged precipitation.

We find that the mixture of high and optically thick clouds represented by the weather state with index ''1'' (WS1) in the ISCCP dataset and considered the most spatially extensive and long-lived type of deep convection is associated with almost half the tropical precipitation, despite occurring only about 6% of the time. This is because its mean precipitation rate at the time of occurrence is about 19 mm day^{-1}, more than 4 times larger than the second most convectively active state (WS2), which happens to also have the second highest mean precipitation rate. The presence of WS1 signifies dynamical conditions that favor stronger precipitation rates: the apparent precipitation of other weather states occurring before or after WS1 in the same grid cell is greater than average. It seems therefore that the precipitation of weather states occurring before or after WS1 reflects its influence on its convective progenitors or descendants. But even this weather state appears to be precipitation-free about half the time according to a frequency distribution analysis of TMPA-3B42 precipitation rates. This is likely an overestimate of rain-free occurrences given the limitations of the rain detection algorithm when precipitation is light and the imperfect spatiotemporal matching. Another feature of WS1 worth mentioning is that it exhibits the strongest seasonal variability among all weather states, still relatively weak on a domain-averaged basis, but with prominent zonal variations that are closely tracked by WS2 (dominated by anvils), but not by WS3 (unorganized convection; the third most convectively active state). When the precipitation data are composited separately over land and ocean grid cells, differences emerge. WS1 precipitates more over ocean, possibly reflecting a combination of factors like a more humid environment preventing extensive evaporation of hydrometeors, larger and slower-moving systems compared to land, and the possibility of biases due to algorithmic differences in the ocean versus land precipitation retrievals. Also, over land, the relative contribution of WS3 to total precipitation goes up significantly, reaching a value close to half that of WS1 (over ocean the relative contribution is closer to a quarter of that of WS1).

The choice of the precipitation dataset used in the compositing affects the results noticeably. The GPCP-1DD precipitation represents the gridcell diurnal average and cannot be combined with ISCCP weather state data available every 3 h without further assumptions. When the same daily precipitation rate is assigned to every weather state that may occur within the grid cell during sunlit hours, the contrast between the three most convective weather states is reduced. The

Unauthenticated | Downloaded 03/23/22 03:38 PM UTC

domain-average precipitation rates and contributions become much more consistent between the two datasets, as might be expected, when most data are discarded in favor of grid cells with a single weather state persisting during daytime. Apparently, for those cases, the GPCP-1DD daily average is a much better representation of the state's precipitation. Diurnally averaged precipitation composites cannot capture as well the frequency of nonprecipitating WS1 occurrences, implying that once WS1 appears in a grid cell, it is very unlikely that the cell will remain precipitation-free for the entire 24-h period.

Since clouds are the most prominent regulators of radiation and precipitation, it is natural to explore in future work the connections between precipitation, radiation, and the state of the atmosphere as a function of cloud regime using a weather state framework. To some extent, work along these lines has already been performed (e.g., Tromeur and Rossow 2010; Gordon and Norris 2010; Tselioudis and Rossow 2011; Oreopoulos and Rossow 2011; and this work), but the unifying effort that will fully integrate the physical relationships between atmospheric dynamical and thermodynamical states and the budgets of radiation and precipitation into a coherent picture has not yet materialized. Once such an effort is completed, a better foundation for how to analyze cloud regimes and associated meteorology in conjunction with energy and water budgets will be available for climate models to capitalize on. This can potentially lead to significant leaps in the quality of model hydrology and energetics.

Acknowledgments. Lazaros Oreopoulos and Dongmin Lee acknowledge funding from NASA's Modeling Analysis and Prediction program and the CloudSat/CALIPSO Science Team recompetition, both managed by Dr. David Considine. William B. Rossow acknowledges funding from the NASA MEASURES and NEWS programs. We thank A. Del Genio for helpful discussions.

REFERENCES

Adler, R. F., and Coauthors, 2003: The Version-2 Global Precipitation Climatology Project (GPCP) monthly precipitation analysis (1979–present). *J. Hydrometeor.,* **4,** 1147–1167.

Anderberg, M. R., 1973: *Cluster Analysis for Applications*. Elsevier, 359 pp.

Casey, S. P. F., A. E. Dessler, and C. Schumacher, 2007: Frequency of tropical precipitating clouds as observed by the Tropical Rainfall Measuring Mission Precipitation Radar and ICESat/Geoscience Laser Altimeter System. *J. Geophys. Res.,* **112,** D14215, doi:10.1029/2007JD008468.

Geerts, B., and T. Dejene, 2005: Regional and diurnal variability of the vertical structure of precipitation systems in Africa based on spaceborne radar data. *J. Climate,* **18,** 893–916.

Gordon, N. D., and J. R. Norris, 2010: Cluster analysis of midlatitude oceanic cloud regimes: Mean properties and temperature sensitivity. *Atmos. Chem. Phys.,* **10,** 6435–6459.

Greenwald, T. J., Y.-K. Lee, J. A. Otkin, and T. L'Ecuyer, 2010: Evaluation of midlatitude clouds in a large-scale high-resolution simulation using CloudSat observations. *J. Geophys. Res.,* **115,** D19203, doi:10.1029/2009JD013552.

Haynes, J. M., C. Jakob, W. B. Rossow, G. Tselioudis, and J. Brown, 2011: Major characteristics of Southern Ocean cloud regimes and their effects on the energy budget. *J. Climate,* **24,** 5061–5080.

Hodges, K. I., and C. D. Thorncroft, 1997: Distribution and statistics of African mesoscale convective weather systems based on the ISCCP Meteosat imagery. *Mon. Wea. Rev.,* **125,** 2821–2837.

Huffman, G. J., R. F. Adler, M. M. Morrissey, D. T. Bolvin, S. Curtis, R. Joyce, B. McGavock, and J. Susskind, 2001: Global precipitation at one-degree daily resolution from multisatellite observations. *J. Hydrometeor.,* **2,** 36–50.

——, and Coauthors, 2007: The TRMM Multisatellite Precipitation Analysis (TMPA): Quasi-global, multiyear, combined-sensor precipitation estimates at fine scales. *J. Hydrometeor.,* **8,** 38–55.

——, R. F. Adler, D. T. Bolvin, and E. J. Nelkin, 2010: The TRMM Multi-satellite Precipitation Analysis (TMPA). *Satellite Applications for Surface Hydrology,* F. Hossain and M. Gebremichael, Eds., Springer-Verlag, 3–22.

Jakob, C., and G. Tselioudis, 2003: Objective identification of cloud regimes in the Tropical Western Pacific. *Geophys. Res. Lett.,* **30,** 2082, doi:10.1029/2003GL018367.

——, and C. Schumacher, 2008: Precipitation and latent heating characteristics of the major tropical western Pacific cloud regimes. *J. Climate,* **21,** 4348–4364.

——, G. Tselioudis, and T. Hume, 2005: The radiative, cloud, and thermodynamic properties of the major tropical western Pacific cloud regimes. *J. Climate,* **18,** 1203–1215.

Lebsock, M. D., C. Kummerow, and G. L. Stephens, 2010: An observed tropical oceanic radiative–convective cloud feedback. *J. Climate,* **23,** 2065–2078.

Machado, L. A. T., and W. B. Rossow, 1993: Structural characteristics and radiative properties of tropical cloud clusters. *Mon. Wea. Rev.,* **121,** 3234–3260.

——, ——, R. L. Guedes, and A. W. Walker, 1998: Life cycle variations of mesoscale convective systems over the Americas. *Mon. Wea. Rev.,* **126,** 1630–1654.

Mekonnen, A., and W. B. Rossow, 2011: The interaction between deep convection and easterly waves over tropical North Africa: A weather state perspective. *J. Climate,* **24,** 4276–4294.

Nesbitt, S. W., and E. J. Zipser, 2003: The diurnal cycle of rainfall and convective intensity according to three years of TRMM measurements. *J. Climate,* **16,** 1456–1475.

Oreopoulos, L., and W. B. Rossow, 2011: The cloud radiative effects of International Satellite Cloud Climatology Project weather states. *J. Geophys. Res.,* **116,** D12202, doi:10.1029/2010JD015472.

Rossow, W. B., and R. A. Schiffer, 1999: Advances in understanding clouds from ISCCP. *Bull. Amer. Meteor. Soc.,* **80,** 2261–2288.

——, G. Tselioudis, A. Polak, and C. Jakob, 2005: Tropical climate described as a distribution of weather states indicated by distinct

Unauthenticated | Downloaded 03/23/22 03:38 PM UTC

mesoscale cloud property mixtures. *Geophys. Res. Lett.,* **32,** L21812, doi:10.1029/2005GL024584.

——, A. Mekonnen, C. Pearl, and W. Goncalves, 2013: Tropical precipitation extremes. *J. Climate,* in press.

Schiffer, R. A., and W. B. Rossow, 1983: The International Satellite Cloud Climatology Project (ISCCP): The first project of the World Climate Research Programme. *Bull. Amer. Meteor. Soc.,* **64,** 779–784.

Susskind, J., P. Piraino, L. Rokke, T. Iredell, and A. Mehta, 1997: Characteristics of the TOVS Pathfinder Path A dataset. *Bull. Amer. Meteor. Soc.,* **78,** 1449–1472.

Tromeur, E., and W. B. Rossow, 2010: Interaction of tropical deep convection with the large-scale circulation in the MJO. *J. Climate,* **23,** 1837–1853.

Tselioudis, G., and W. B. Rossow, 2011: Time scales of variability of the tropical atmosphere derived from cloud-defined weather states. *J. Climate,* **24,** 602–608.

Williams, K. D., and M. J. Webb, 2008: A quantitative performance assessment of cloud regimes in climate models. *Climate Dyn.,* **33,** 141–157.

Zhang, Y., S. Klein, G. G. Mace, and J. Boyle, 2007: Cluster analysis of tropical clouds using CloudSat data. *Geophys. Res. Lett.,* **34,** L12813, doi:10.1029/2007GL029336.

——, ——, J. Boyle, and G. G. Mace, 2010: Evaluation of tropical cloud and precipitation statistics of Community Atmosphere Model version 3 using CloudSat and CALIPSO data. *J. Geophys. Res.,* **115,** D12205, doi:10.1029/2009JD012006.

Unauthenticated | Downloaded 03/23/22 03:38 PM UTC